RESEARCH ARTICLE

Molecular and Genetic Characterization of MHC Deficiency Identifies EZH2 as Therapeutic Target for Enhancing Immune Recognition

Daisuke Ennishi[1], Katsuyoshi Takata[1], Wendy Béguelin[2], Gerben Duns[1], Anja Mottok[3], Pedro Farinha[1], Ali Bashashati[4], Saeed Saberi[4], Merrill Boyle[1], Barbara Meissner[1], Susana Ben-Neriah[1], Bruce W. Woolcock[1], Adèle Telenius[1], Daniel Lai[4], Matt Teater[2], Robert Kridel[1], Kerry J. Savage[1], Laurie H. Sehn[1], Ryan D. Morin[5], Marco A. Marra[6], Sohrab P. Shah[4], Joseph M. Connors[1], Randy D. Gascoyne[1], David W. Scott[1], Ari M. Melnick[2], and Christian Steidl[1]

ABSTRACT We performed a genomic, transcriptomic, and immunophenotypic study of 347 patients with diffuse large B-cell lymphoma (DLBCL) to uncover the molecular basis underlying acquired deficiency of MHC expression. Low MHC-II expression defines tumors originating from the centroblast-rich dark zone of the germinal center (GC) that was associated with inferior prognosis. MHC-II–deficient tumors were characterized by somatically acquired gene mutations reducing MHC-II expression and a lower amount of tumor-infiltrating lymphocytes. In particular, we demonstrated a strong enrichment of *EZH2* mutations in both MHC-I– and MHC-II–negative primary lymphomas, and observed reduced MHC expression and T-cell infiltrates in murine lymphoma models expressing mutant *Ezh2*^{Y641}. Of clinical relevance, EZH2 inhibitors significantly restored MHC expression in *EZH2*-mutated human DLBCL cell lines. Hence, our findings suggest a tumor progression model of acquired immune escape in GC-derived lymphomas and pave the way for development of complementary therapeutic approaches combining immunotherapy with epigenetic reprogramming.

SIGNIFICANCE: We demonstrate how MHC-deficient lymphoid tumors evolve in a cell-of-origin–specific context. Specifically, *EZH2* mutations were identified as a genetic mechanism underlying acquired MHC deficiency. The paradigmatic restoration of MHC expression by EZH2 inhibitors provides the rationale for synergistic therapies combining immunotherapies with epigenetic reprogramming to enhance tumor recognition and elimination.

See related commentary by Velcheti et al., p. 472.

INTRODUCTION

Immune escape represents one of the major hallmarks of cancer, including lymphoma (1). Among the tumor immune escape mechanisms described to date, alterations in the expression of MHC molecules mainly facilitate immune evasion due to their major role in antigen presentation to T lymphocytes and the regulation of natural killer (NK) cell function (2, 3). The majority of cancer immunotherapies, including immune-checkpoint inhibitors, aim to counteract immune evasion by shifting the balance in favor of immune activation, enabling T or NK cell–mediated cancer cell elimination (4, 5). Of clinical relevance, it has been reported that downregulation of MHC molecules on the cell membrane reduces immune reactivity against tumors and results in reduced efficacy and unfavorable clinical outcomes of cancer immunotherapies (6–9). However, the molecular and genetic mechanisms underlying the deficiency of MHC expression remain poorly understood.

Although the frequency of MHC loss of expression is variable according to cancer type, the frequency in diffuse large B-cell lymphoma (DLBCL) is known to be relatively high; MHC-I and MHC-II are lost in 40% to 60% and 20% to 40% of DLBCL cases, respectively (10–13). DLBCL, representing the most common lymphoma subtype, is recognized for two major subtypes based on cell of origin (COO), referred to as the Activated B cell–like (ABC) subtype and Germinal Center B cell–like (GCB) subtype, which have distinct underlying biology and clinical behavior (14, 15). Although the mechanism and outcome of immune evasion may be variable between COO subtypes, almost nothing is known about whether and how COO subtypes affect the interaction between MHC expression and the tumor immune microenvironment and clinical outcome.

The most recent genomic landscape studies suggested a strong link between somatic gene mutations and COO derivation that define subtype-specific gene clusters (16–18); however, tumor microenvironment biology and related therapeutic targeting remain a gaping hole in these studies. Here, we conducted genetic, transcriptomic, and multilayered immune-cell profiling using 347 DLBCL specimens derived from a population-based cohort. Our study comprehensively characterizes MHC expression in the context of COO and derivation from centroblasts and centrocytes within germinal centers (GC) in particular. We demonstrate that B cells with low MHC-II expression acquired genetic alterations to further reduce MHC-II expression, which alters the T-cell landscape to tumor-preferable microenvironments. This analysis uncovered a significant enrichment of *EZH2* mutations in the MHC-deficient cases and established a functional link between *EZH2* mutations and loss of MHC-I and MHC-II expression. By showing that EZH2 inhibitors can restore MHC expression in human *EZH2*-mutant DLBCL cells, we provide important insights for the development of complementary approaches for MHC upregulation in the context of modern immunotherapies.

[1]Centre for Lymphoid Cancer, British Columbia Cancer, Vancouver, British Columbia, Canada. [2]Division of Hematology/Oncology, Department of Medicine, Weill Cornell Medical College, New York, New York. [3]Institute of Human Genetics, Ulm University and Ulm University Medical Center, Ulm, Germany. [4]Molecular Oncology, British Columbia Cancer, Vancouver, British Columbia, Canada. [5]Department of Molecular Biology and Biochemistry, Simon Fraser University, Burnaby, British Columbia, Canada. [6]Genome Science Centre, British Columbia Cancer, Vancouver, British Columbia, Canada.

Note: Supplementary data for this article are available at Cancer Discovery Online (http://cancerdiscovery.aacrjournals.org/).

D. Ennishi and K. Takata contributed equally to this article.

Corresponding Author: Christian Steidl, British Columbia Cancer Research Centre, 675 West 10th Avenue, Room 12-110, Vancouver, BC V5Z 1L3, Canada. Phone: 604-675-8046; Fax: 604-675-8183; E-mail: CSteidl@bccancer.bc.ca

doi: 10.1158/2159-8290.CD-18-1090

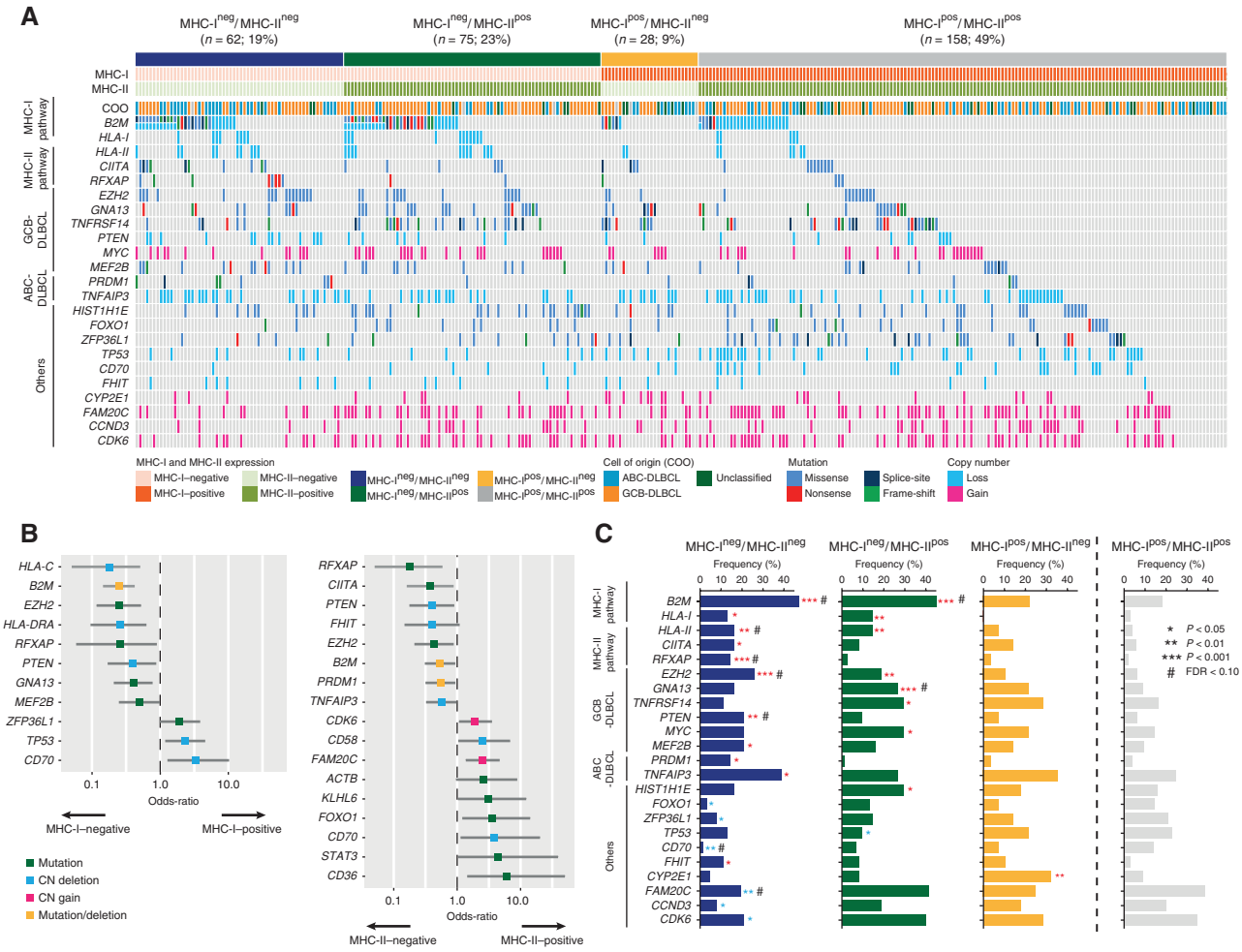

Figure 1. Recurrent mutation and copy-number alterations (CNA) associated with loss of MHC-I and MHC-II expression. **A,** Spectrum of genetic alterations (GA) including mutations and CNAs which are significantly enriched in the cases with either MHC-I or MHC-II loss of expression. Top bar represents the MHC expression pattern. **B,** Forest plots summarize the results of Fisher exact tests analyzing the enrichment of GAs by MHC-I (left) and MHC-II (right). Only significantly enriched genes in either MHC-positive or MHC-negative cases ($P < 0.05$) are represented. ORs and 95% confidence intervals are shown. The color of box represents the type of GAs. **C,** Bar plots show the frequencies of GAs within four subgroups by the pattern of MHC expression status. Colored asterisks (red, positive association; blue, negative association) represent significant difference of frequencies of each subgroup compared with MHC-I and MHC-II double-positive cases.

RESULTS

Patterns and Frequency of MHC Class I and Class II Protein Expression and Association with COO Subtype

We first characterized the MHC-I and MHC-II expression status in 347 DLBCL cases (Supplementary Table S1). We found the following MHC-I and MHC-II staining patterns: membrane-positive [n = 188 (57%) and n = 233 (72%), respectively], cytoplasmic only–positive/membrane-negative [n = 86 (26%) and 31 (10%), respectively], and negative for both membrane and cytoplasmic [n = 55 (17%) and n = 59 (18%), respectively; Supplementary Fig. S1A–S1F; Supplementary Table S2]. Overall, membranous MHC-I and MHC-II expression was not detected in 141 of 329 (43%) and 90 of 323 (28%) cases, respectively, which was considered as "loss of MHC expression" for further analysis, as a direct contact between antigen-presenting cells (APC) and effector cells is established only when MHC is expressed on the cell surface. Importantly, mRNA expression significantly correlated with protein expression status for both MHC-I ($P = 0.04$) and MHC-II ($P = 2.30E{-}10$). Although the frequency of loss of MHC-I expression was not significantly different between COO subtypes, loss of MHC-II expression occurred more often in ABC-DLBCL consistent with previous studies (36% vs. 22%, $P = 0.03$; Supplementary Fig. S1G; refs. 19, 20). Of note, concurrent loss of MHC-I and MHC-II expression was observed in 19% (62/323) of DLBCL, and the frequency of the cases with isolated MHC-I loss was more common than that of isolated MHC-II loss (23% and 9%, respectively; Fig. 1A; Supplementary Fig. S1H; Supplementary Table S3).

Mutational Patterns Associated with MHC Expression Status

The molecular and genetic basis underlying loss of MHC-I and MHC-II expression is largely unknown. Therefore, we

first investigated the enrichment of somatic genetic alterations in tumors with MHC loss of expression (Fig. 1A). For this analysis, we cataloged the genetic alterations using deep, targeted amplicon sequencing (n = 57 genes), genome-wide SNP6 array, and RNA sequencing (RNA-seq) in 347 DLBCL cases. As expected, we observed recurrent mutations in the antigen presentation machinery, including HLA genes and *B2M*, in the cases with MHC-I loss of expression (both, $P < 0.001$). In addition, we identified that mutations of *EZH2, GNA13*, and *MEF2B*, as well as *PTEN* deletions, were significantly associated with MHC-I loss ($P < 0.001$, $P = 0.004$, $P = 0.04$, and $P = 0.02$, respectively). In contrast, deletions of *CD70* and *TP53* were significantly associated with positive expression of MHC-I ($P = 0.007$ and $P = 0.008$, respectively; Fig. 1B; Supplementary Table S4).

We also found that mutations of *RFXAP* and *CIITA*, components of the MHC-II enhanceosome, were significantly enriched in the cases with MHC-II loss ($P = 0.002$ and $P = 0.02$, respectively). Genetic alterations specific to ABC-DLBCL, such as those in *PRDM1* and *TNFAIP3*, were also more frequently observed in the cases with loss of MHC-II expression ($P = 0.003$ and $P = 0.03$, respectively), reflecting the reduced expression of MHC-II in ABC-DLBCL (19). Interestingly, *EZH2* mutation and *PTEN* deletions were significantly enriched in the cases with loss of MHC-II expression (both, $P = 0.02$), which were similarly observed in MHC-I–negative DLBCL (Fig. 1B; Supplementary Table S5).

In addition, we analyzed the recurrent genetic alterations in the cases with concurrent loss of MHC-I and MHC-II expression, demonstrating that *EZH2* mutation was strongly enriched compared with double-positive cases ($P = 0.0003$; Fig. 1C). Importantly, the association between *EZH2* mutation and loss of MHC-I and MHC-II expression was more evident when the analysis was restricted to GCB-DLBCL ($P = 1.21E{-}04$ and $P = 1.02E{-}04$, respectively). Altogether, our genetic analyses highlight the strong enrichment of *EZH2* mutations in DLBCL cases with loss of MHC-I and MHC-II expression.

MHC Class II Expression Defines a Distinct Molecular Subtype with Unique COO within GCB-DLBCL

Next, we performed gene expression profiling to elucidate the molecular mechanism underlying acquired loss of MHC expression. Surprisingly, hundreds of genes were differentially expressed (FDR < 0.05) according to MHC-II status in GCB-DLBCL, whereas only 4 genes (*HLA-DMA, -DRA, -DPA1*, and *CD74*) were differentially expressed in ABC-DLBCL. We also found that only a few genes were differentially expressed according to MHC-I expression in both COO subtypes (Fig. 2A). These results suggest that MHC-II expression is part of a more global transcriptomic profile in GCB-DLBCL that prompted us to investigate the biological processes associated with MHC-II deficiency in the GCB subtype.

A total of 664 genes were differentially expressed, including 285 upregulated and 379 downregulated genes in MHC-II–negative GCB-DLBCL cases (Supplementary Table S6). As expected, the HLA-associated and regulating genes *CIITA, RFXAP,* and *CD74* were upregulated in MHC-II–positive cases. Of interest, several genes involved in the migration and differentiation of GC B-cell between the centroblast-rich dark zone (DZ) and centrocyte-rich light zone (LZ) were found as the most highly ranked genes in differential expression analysis supervised by MHC-II expression status (e.g., *CD83, CD40LG, IRF4, CD80,* and *BATF*; Fig. 2B). This finding suggests that MHC-II–positive and MHC-II–negative tumors within GCB-DLBCL are closely related to LZ and DZ B cells, respectively. In order to validate this finding, we performed gene set enrichment analysis (GSEA), showing the significant enrichment of DZ and LZ gene signatures (21) in MHC-II–negative and MHC-II–positive cases, respectively (both FDR < 0.0001; Fig. 2C). In addition, pathway enrichment analysis (PEA) revealed that the mismatch repair pathway was ranked as the top gene ontology term (FDR < 0.0001) in MHC-II–negative cases (Supplementary Table S7). The top component genes significantly enriched in this pathway involve *MSH2* and *MSH6*, which are associated with the transition from naïve B cells to centroblasts (22), and also are required to produce mutations within the immunoglobulin V region during somatic hypermutation (23). Collectively, these results demonstrate that MHC-II expression is a surrogate marker that can further subdivide GCB-DLBCL into two molecular subtypes with distinct COO corresponding to centroblasts and centrocytes.

Genetic correlative analysis within GCB-DLBCL also revealed that mutations affecting *RFXAP* and *CIITA* were significantly enriched in MHC-II–negative cases ($P = 0.003$ and $P = 0.01$, respectively), which may further decrease the surface MHC-II levels on tumor B cells due to their role in repressing MHC-II surface expression (24, 25). Strikingly, *CD83* mutations, which elevate and stabilize MHC-II expression on centrocytes (21, 26), were significantly enriched in MHC-II–positive GCB-DLBCL ($P = 0.008$; Supplementary Fig. S2A–S2B).

Collectively, we observed the distinct molecular features associated with MHC-II expression in GCB-DLBCL (Fig. 3A). Notably, MHC-II surface levels and degradation are dynamically regulated in nontumor GC B cells, where MHC-II expression is relatively lower in centroblasts and higher in centrocytes (21, 26). Thus, genetic alterations selectively acquired in tumors originating from DZ and LZ B cells might enhance the difference of surface MHC-II expression (Fig. 3B).

Outcome Correlates of MHC Class I and II Expression

Analysis of the prognostic significance of MHC-I and MHC-II expression in the entire DLBCL cohort as well as within each COO subtype revealed significant correlations of MHC-II expression with time to progression (TTP) in either COO subtype (Fig. 3C; Supplementary Table S8). However, surprisingly, MHC-II negativity by IHC was significantly correlated with unfavorable outcomes in GCB-DLBCL, whereas an opposite prognostic impact, i.e., favorable outcomes, was found in ABC-DLBCL. Cox proportional hazards model, controlling for International Prognostic Index (IPI) parameters, revealed that the prognostic effect of MHC-II loss is independent of IPI (Supplementary Table S9).

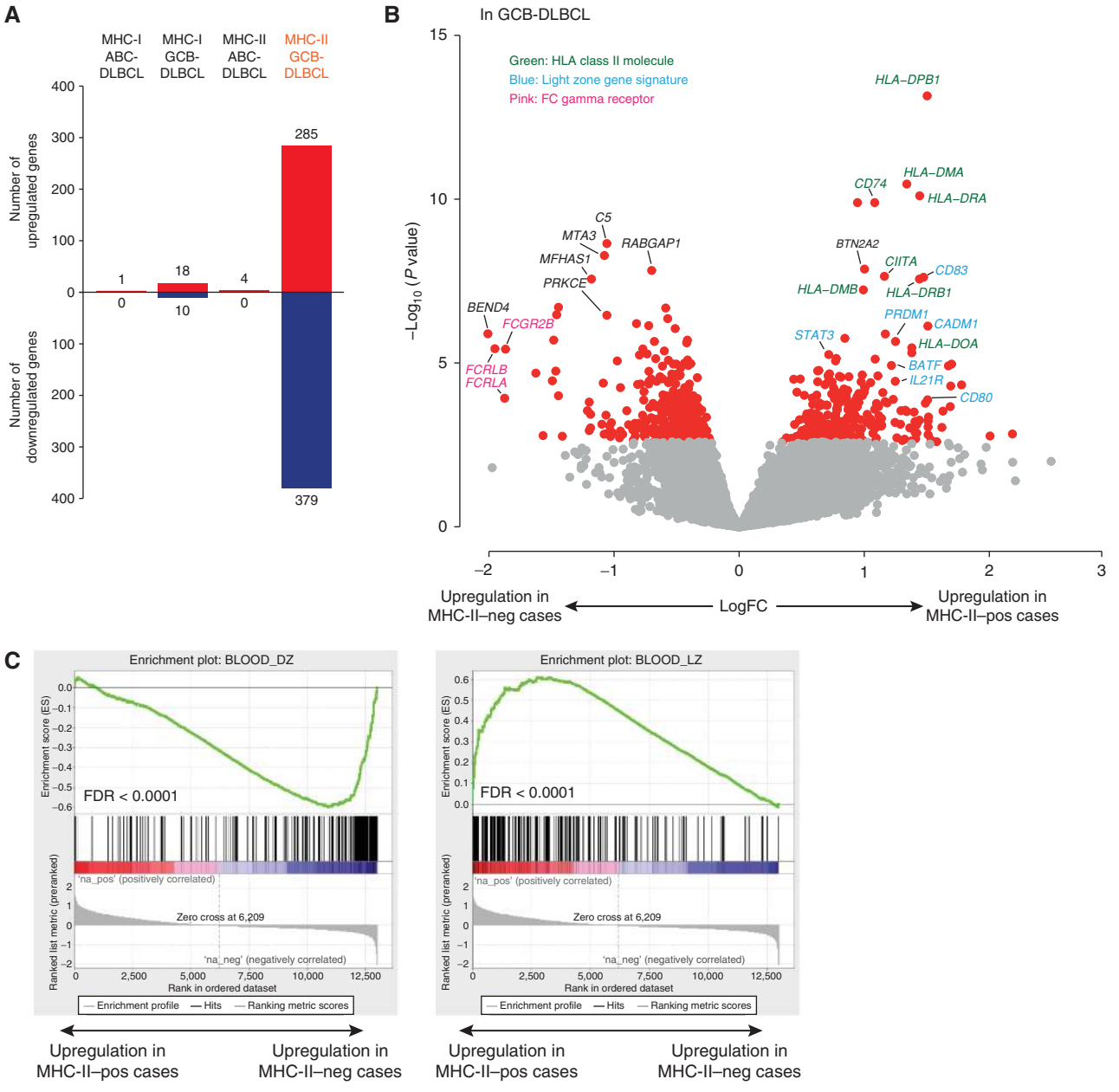

Figure 2. Gene expression profiling reveals the distinct molecular features of GCB-DLBCL cases defined by MHC-II expression. **A,** Bar plot (red, upregulation; blue, downregulation, in MHC-negative cases) shows the genes significantly differentially expressed (FDR < 0.05) according to MHC expression status; (i) MHC-I–positive ($n = 63$) vs. MHC-I–negative ($n = 41$) ABC-DLBCLs, (ii) MHC-II–positive ($n = 67$) vs. MHC-II–negative ($n = 37$) ABC-DLBCLs, (iii) MHC-I–positive ($n = 95$) vs. MHC-I–negative ($n = 86$) GCB-DLBCLs, and (iv) MHC-II–positive ($n = 136$) vs. MHC-II–negative ($n = 40$) GCB-DLBCLs. **B,** Volcano plot of differences of gene expression between MHC-II–negative and MHC-II–positive GCB-DLBCL [*x* axis; $\log_2$ fold change (FC) of difference] and significance (*y* axis). Red dots show the genes with significant difference (FDR < 0.05). **C,** GSEA plots illustrating the enrichment for DZ-upregulated gene signature (top) and LZ-upregulated gene signature (bottom; ref. 21) in our gene expression data according to MHC-II expression.

MHC Class II Expression Alters Immune Activity and T-cell Infiltration in a COO-Dependent Manner

We next investigated the effects of MHC expression on immune activity and/or immune-cell infiltrates in the tumor microenvironment. By quantifying immune cells with flow cytometry, *in silico* methods using gene expression profiling, and a digital scoring system using IHC staining on tissue microarrays (TMA) in the same cases, we found a significant increase in the fraction of $CD8^+$ and $CD4^+$ T cells in MHC-positive tumors compared with MHC-negative tumors in GCB-DLBCL (Fig. 4A). In contrast, we did not detect any significant differences in major T-cell populations according to MHC expression in ABC-DLBCL, indicating that the effect of MHC expression on the immune-cell microenvironment

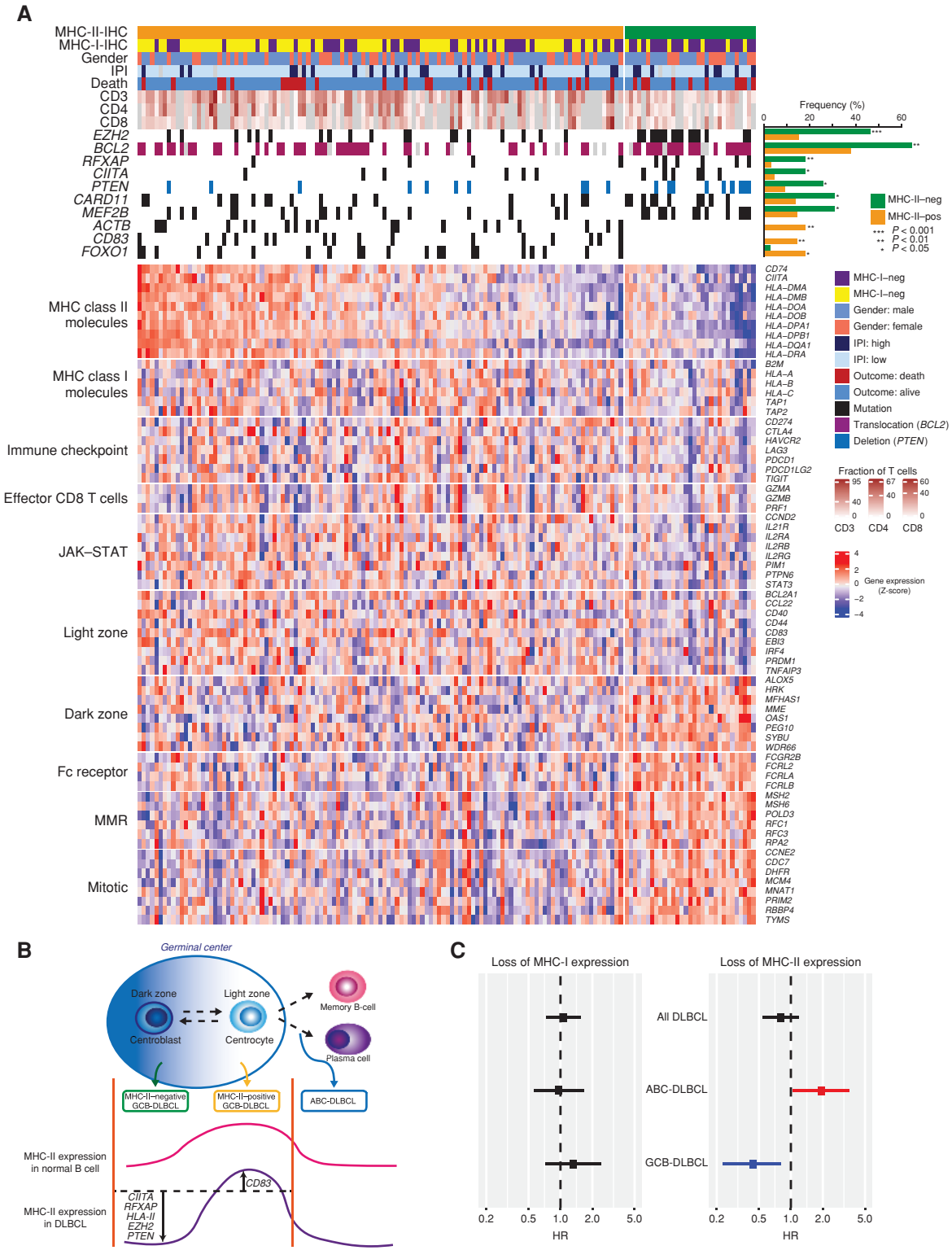

Figure 3. Association between MHC-II expression and clinical and molecular features in GCB-DLBCL. **A,** Heatmap shows the MHC-I expression status, clinical information (gender, IPI, and death), flow cytometry data (CD3, 4, and 8 fractions), genetic alterations (color represents the type of GAs), and gene expression grouped by pathway. MHC-II expression status is represented at top bar. Top right, Bar plots show the frequencies of GAs and comparison between MHC-II–negative (green) and MHC-II–positive (orange) cases. **B,** Schematic model. Change of MHC-II expression during normal B-cell differentiation stage and corresponding tumor B cells. **C,** Forest plots summarize the prognostic effects of loss of expression of MHC-I (left) and MHC-II (right) in all DLBCL, ABC-DLBCL, and GCB-DLBCL. HRs and 95% confidence intervals are shown. Highlighted boxes and bars represent significant effect with TTP (blue, unfavorably prognostic; red, favorably prognostic).

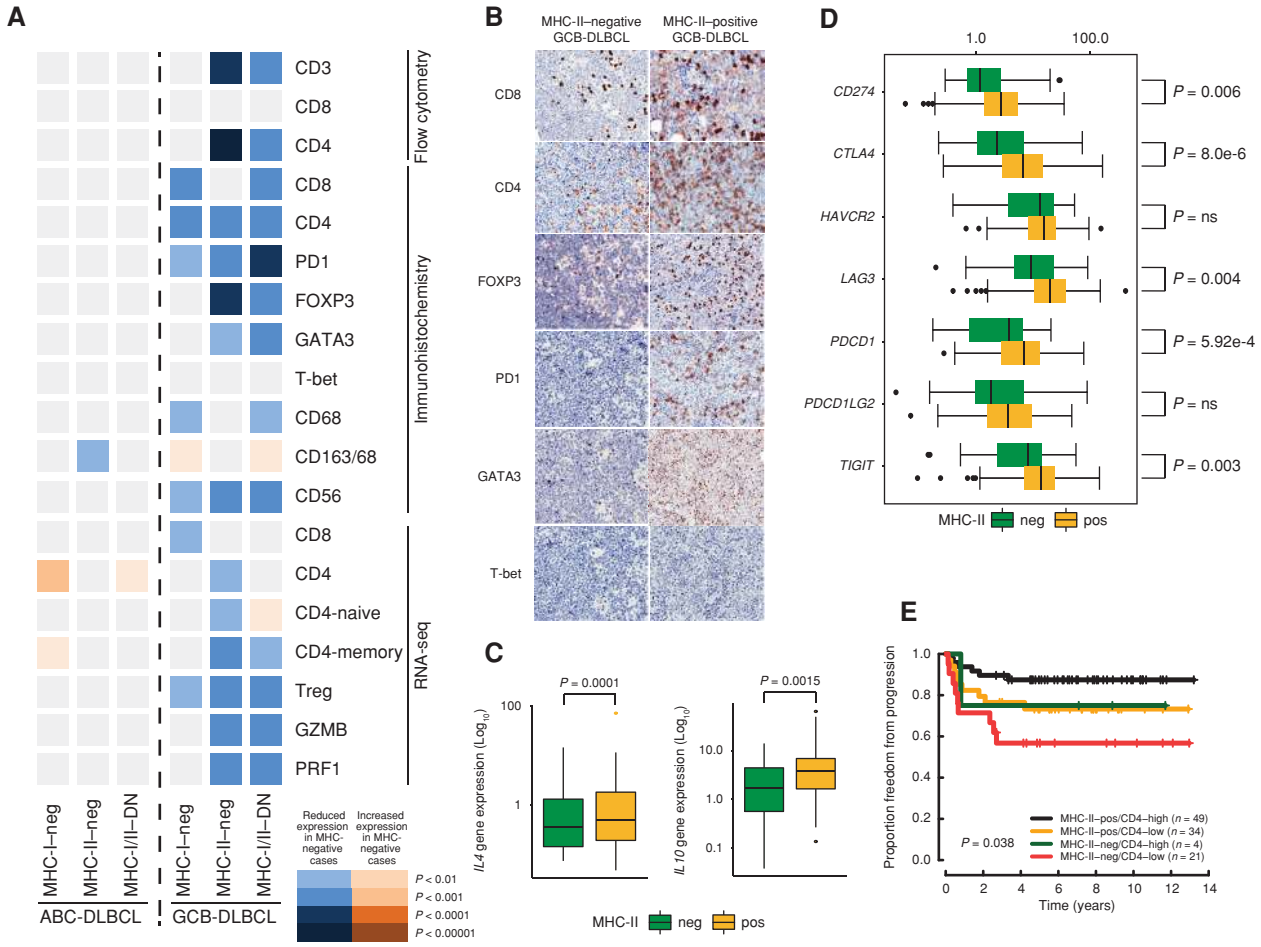

Figure 4. Difference of tumor immune microenvironment composition according to MHC-II expression. **A,** Heat map representing the differences of immune-cell fraction according to MHC expression (Wilcoxon rank-sum test). Immune-cell fractions are defined by IHC, flow cytometry, and deconvolution using RNA-seq. Increase of an immune-cell subset among MHC-negative cases is shown in red, and a decrease is shown in blue. DN, double negative. **B,** IHC staining for major immune cells in MHC-II–negative (left) and MHC-II–positive (right) GCB-DLBCL (magnification, ×20). **C** and **D,** Gene expression of IL4 and IL10 (**C**) and immune-checkpoint genes (**D**), according to MHC-II expression status (MHC-II–positive, $n = 136$ cases; MHC-II–negative, $n = 40$ cases). **E,** Kaplan–Meier curves according to the combined MHC-II expression status and CD4$^+$ T-cell counts.

is COO-dependent. We also observed stronger correlations of MHC-II expression with the amount of tumor-infiltrating lymphocytes (TIL) measured by CD3$^+$ T cells compared with MHC-I expression (P = 2.3E–05 vs. P = 0.27, respectively; Fig. 4A). Moreover, cytolytic activity, measured by the levels of two genes, granzyme B (*GZMB*) and perforin (*PRF1*), was significantly correlated with MHC-II expression (P = 0.004 and P = 0.006, respectively), but not with MHC-I, suggesting a critical role of MHC-II for the interface with immune cells in the tumor microenvironment in GCB-DLBCL. Interestingly, the amount of NK cells defined by CD56-IHC was significantly reduced in MHC-I–negative cases (P = 0.005), a finding that was more evident in GCB-DLBCL compared with ABC-DLBCL (Fig. 4A).

We next explored which subsets of T cells were highly affected by loss of MHC-II expression in GCB-DLBCL. Characterization of CD4$^+$ T-cell subsets showed a marked difference of the number of PD-1$^+$ and FOXP3$^+$ T cells between MHC-II–positive and MHC-II–negative tumors (P = 0.001 and P = 4.3E–05, respectively; Fig. 4A and B). Consistent with these IHC results, *in silico* deconvolution analysis from RNA-seq also revealed that MHC-II loss was significantly associated with a reduction of regulatory T cells (P = 0.002). Interestingly, *GATA3*, which is a marker of the Th2 anti-inflammatory phenotype, was also significantly lower in MHC-II–negative GCB-DLBCL (P = 0.01), whereas the amount of Th1 cells with T-bet (*TBX21*) expression was not changed by MHC-II expression loss. To further assess the Th1/Th2 polarization associated with MHC-II expression, we studied gene expression of cytokines and chemokines (Supplementary Fig. S3). Representative Th2-type cytokines, such as *IL4* and *IL10*, were significantly associated with MHC-II expression in GCB-DLBCL, whereas there were no correlations of Th1-type cytokines, including *IL12* and *CCR5*, with MHC-II expression (Fig. 4C).

To further characterize markers of T-cell exhaustion in association with MHC-II expression, we analyzed RNA-seq

data of genes encoding for immune-checkpoint proteins (e.g., CTLA4, PD-1, and TIGIT). We found significantly increased gene expression of immune-checkpoint proteins in MHC-II–positive cases (Fig. 4D). In particular, *CTLA4* and *PDCD1* expressions were much higher ($P = 0.0004$ and $P = 0.0005$, respectively) in MHC-II–positive cases compared with MHC-II–negative cases. Of importance, these associations were not found in ABC-DLBCL (Supplementary Fig. S4). Overall, these results suggest that MHC-II expression on tumor cells maintains the cross-talk with effector T cells in GCB-DLBCL characterized by abundant TILs with elevated cytotoxic activity, but also regulatory T cells limiting an active immune response.

We also analyzed the prognostic effect of the amount of $CD4^+$ and $CD8^+$ T cells in the tumor microenvironment, showing that lower amounts of $CD4^+$ T cells are significantly associated with worse outcome, particularly in GCB-DLBCL, whereas no prognostic impact was found for $CD8^+$ T cells (Supplementary Table S8). We further assessed the combined prognostic effect of MHC-II and $CD4^+$ T cells, and, as expected, the poorest outcome group was defined by concurrent loss of MHC-II expression and low $CD4^+$ T cells in GCB-DLBCL (Fig. 4E).

EZH2 Mutation Is Linked to Loss of MHC Expression and a Reduced T-cell Infiltrate in the Tumor Microenvironment

Our genetic and molecular analyses highlighted the strong enrichment of *EZH2* mutations in patients with DLBCL with loss of MHC-I and MHC-II expression (Fig. 1). Indeed, 77% of *EZH2*-mutated cases lost either MHC-I and/or MHC-II expression in DLBCL (Fig. 5A). Interestingly, three cases with atypical *EZH2* mutations were also negative for both MHC-I and MHC-II expression (Supplementary Table S10). In MHC-II–negative GCB-DLBCL, the subgroup showing poor outcome and low TILs, *EZH2* is the most frequently mutated gene with the highest statistical significance ($P = 1.23E{-}05$; Supplementary Fig. S2B). In addition, *EZH2* mutation demonstrated the most significant association with loss of MHC-I ($P = 1.01E{-}05$; Supplementary Fig. S2A) among all evaluated genes in GCB-DLBCL. We also found a mutually exclusive pattern between *EZH2* mutation and deletions of the MHC-I and MHC-II loci ($P = 0.06$ and $P = 0.02$, respectively). Furthermore, significantly reduced cytolytic activity was observed in *EZH2*-mutated cases (Fig. 5B). Collectively, these findings suggest a critical role

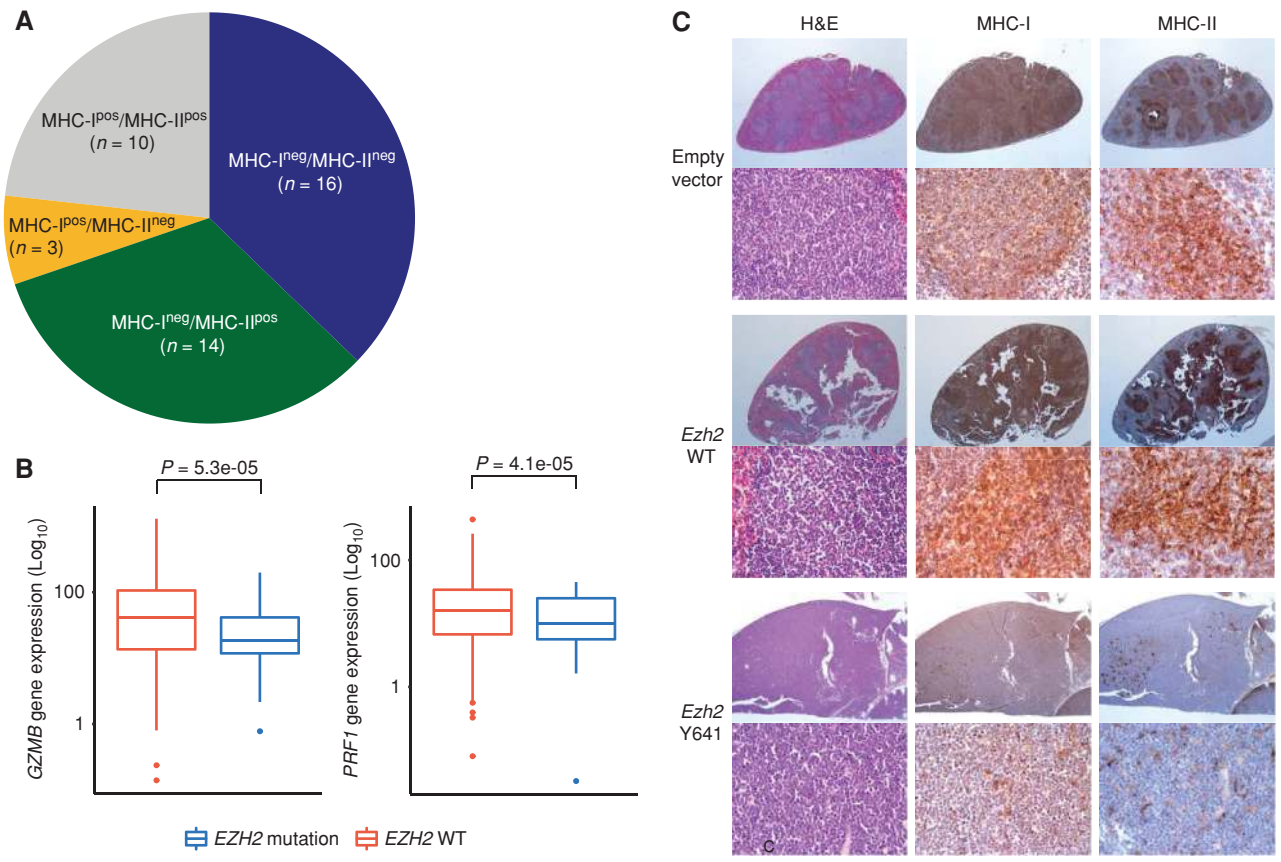

Figure 5. Association of *EZH2* mutation with MHC-I and MHC-II expression and TILs in *Ezh2/VavP-Bcl2* transgenic murine model. **A,** Staining pattern of MHC-I and MHC-II expression in *EZH2*-mutated DLBCL cases. **B,** Comparison of gene expression of cytolytic activity according to *EZH2* mutation status. **C,** Splenic and/or lymph node tissues from EV, WT *Ezh2*, and mutant *Ezh2* mice were stained with hematoxylin and eosin (H&E), MHC-I, and MHC-II (top and bottom of each plot: magnification ×2 and ×40, respectively). (*continued on next page*)

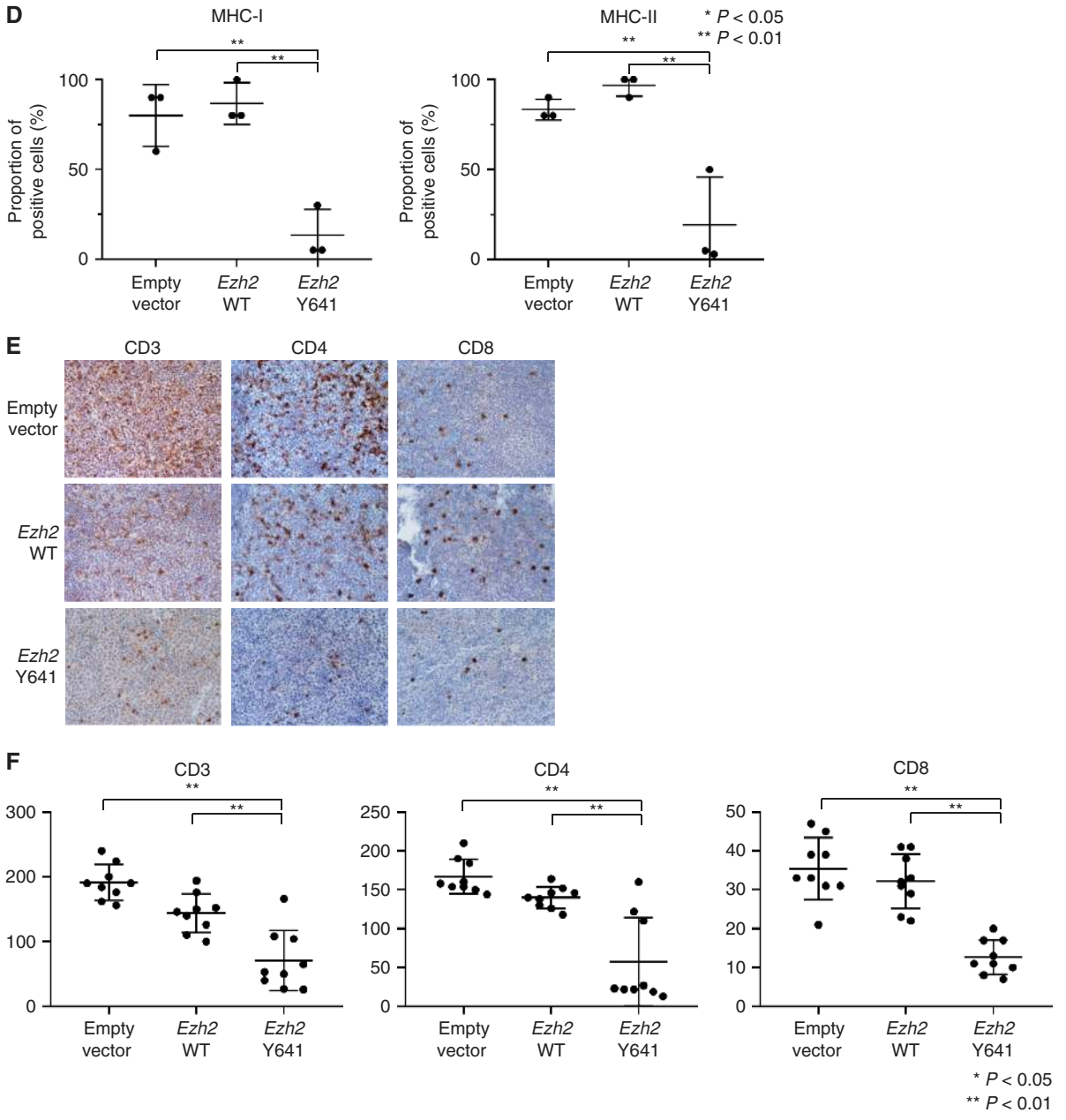

Figure 5. ***(Continued)*** **D,** Comparisons of proportion of MHC-I–positive (left) and MHC-II–positive (right) cells between EV, WT *Ezh2*, and mutant *Ezh2* mice. **E** and **F,** Tissues from EV, WT *Ezh2*, and mutant *Ezh2* mice were stained with CD3, CD4, and CD8 (magnification, ×40; **E**) and comparison of proportions of positive cells (**F**).

of *EZH2* mutation in regulating MHC expression and contributing to immune microenvironment biology. Thus, we investigated in more detail the functional consequences of *EZH2* mutations for loss of MHC expression using murine models and human lymphoma cell lines.

To experimentally confirm decreased MHC expression induced by *EZH2* Y641 mutations, we measured surface MHC-I and MHC-II expression on tumor B cells using an *Ezh2*-mutant mouse model system, which was previously established (27). Mice were transplanted with *VavP-Bcl2* bone marrow infected with mutant *Ezh2*, wild-type (WT) *Ezh2*, or empty vector (EV). This model system had been intensively evaluated in histopathologic examination, by clonality analysis, and for tumor burden and survival of mice (27). Using this mouse model, we have stained MHC-I and MHC-II expression of tumors and observed significantly reduced expression of both MHC-I and MHC-II in mutant *Ezh2* mouse tumors compared with WT *Ezh2* and EV mice (both, $P < 0.01$; Fig. 5C and D). Moreover, the amounts of $CD3^+$, $CD4^+$, and $CD8^+$ T cells were all significantly reduced in mutant *Ezh2* tumors (all, $P < 0.01$; Fig. 5E and F).

In order to further validate these findings in a second model, we measured surface MHC-I and MHC-II expression on tumor B cells in *Ezh2*^{Y641N} or *Ezh2*^{Y641F} (*Ezh2*$^{Y641F/N}$) mutant and WT mice crossed to mice with constitutive expression of *Bcl2*. For these analyses, we generated a conditional Cγ1Cre; *Ezh2*$^{Y641F/N}$/*VavP-Bcl2* murine model which develops B-cell lymphomas resembling human DLBCL. Histopathologic examination of spleens and/or lymph nodes revealed that most of the tumor B cells in *VavP-Bcl2* mice expressed both MHC-I and MHC-II on their surface. In sharp contrast, tumor cells in Cγ1Cre; *Ezh2*$^{Y641F/N}$/*VavP-Bcl2* mice presented very weak or no expression of MHC-I and MHC-II (Fig. 6A). We also measured the proportion of MHC-positive cells, showing significant reduction of tumor B cells expressing MHC-I and MHC-II in Cγ1Cre; *Ezh2*$^{Y641F/N}$/*VavP-Bcl2* mice compared with *VavP-Bcl2* mice ($P = 0.02$ and $P = 0.04$, respectively; Fig. 6B). In addition, a significantly reduced T-cell infiltrate was observed in Cγ1Cre; *Ezh2*$^{Y641F/N}$/*VavP-Bcl2* mice as well (CD3, CD4, and CD8, $P < 0.01$; Fig. 6C and D), which again demonstrates

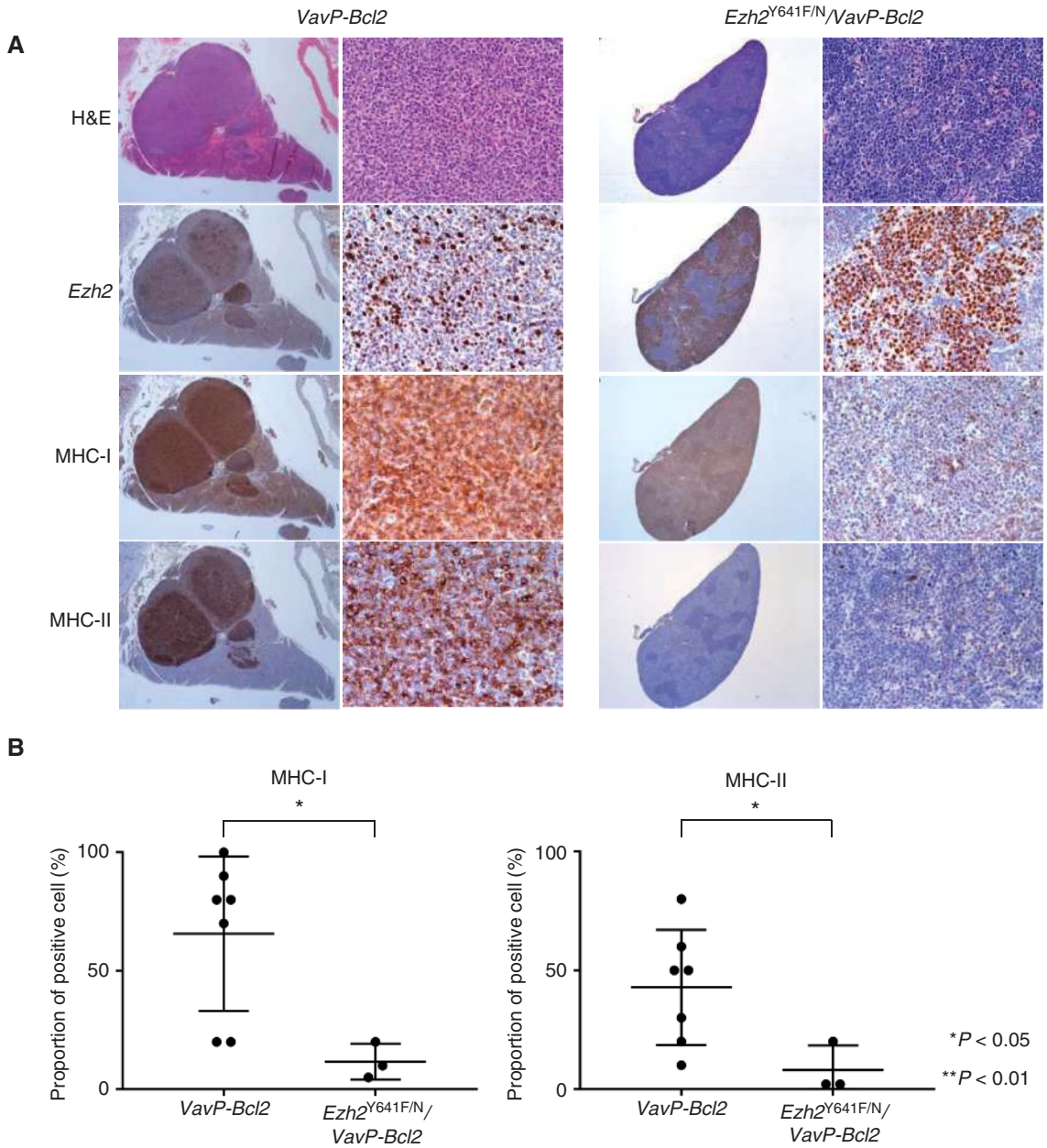

Figure 6. Association of *EZH2* mutation with MHC-I and MHC-II expression and TILs in *Ezh2*$^{Y641F/N}$/*VavP-Bcl2* mouse model. **A,** Splenic and/or lymph node tissues from *Ezh2* WT/*VavP-Bcl2* and *Ezh2*$^{Y641F/N}$/*VavP-Bcl2* mice were stained with hematoxylin and eosin (H&E), EZH2, MHC-I, and MHC-II (left and right side of each plot: magnification ×2 and ×40, respectively). **B,** Comparisons of proportion of MHC-I–positive (top) and MHC-II–positive (bottom) cells between *Ezh2* WT/*VavP-Bcl2* and *Ezh2*$^{Y641F/N}$/*VavP-Bcl2* mice. (*continued on next page*)

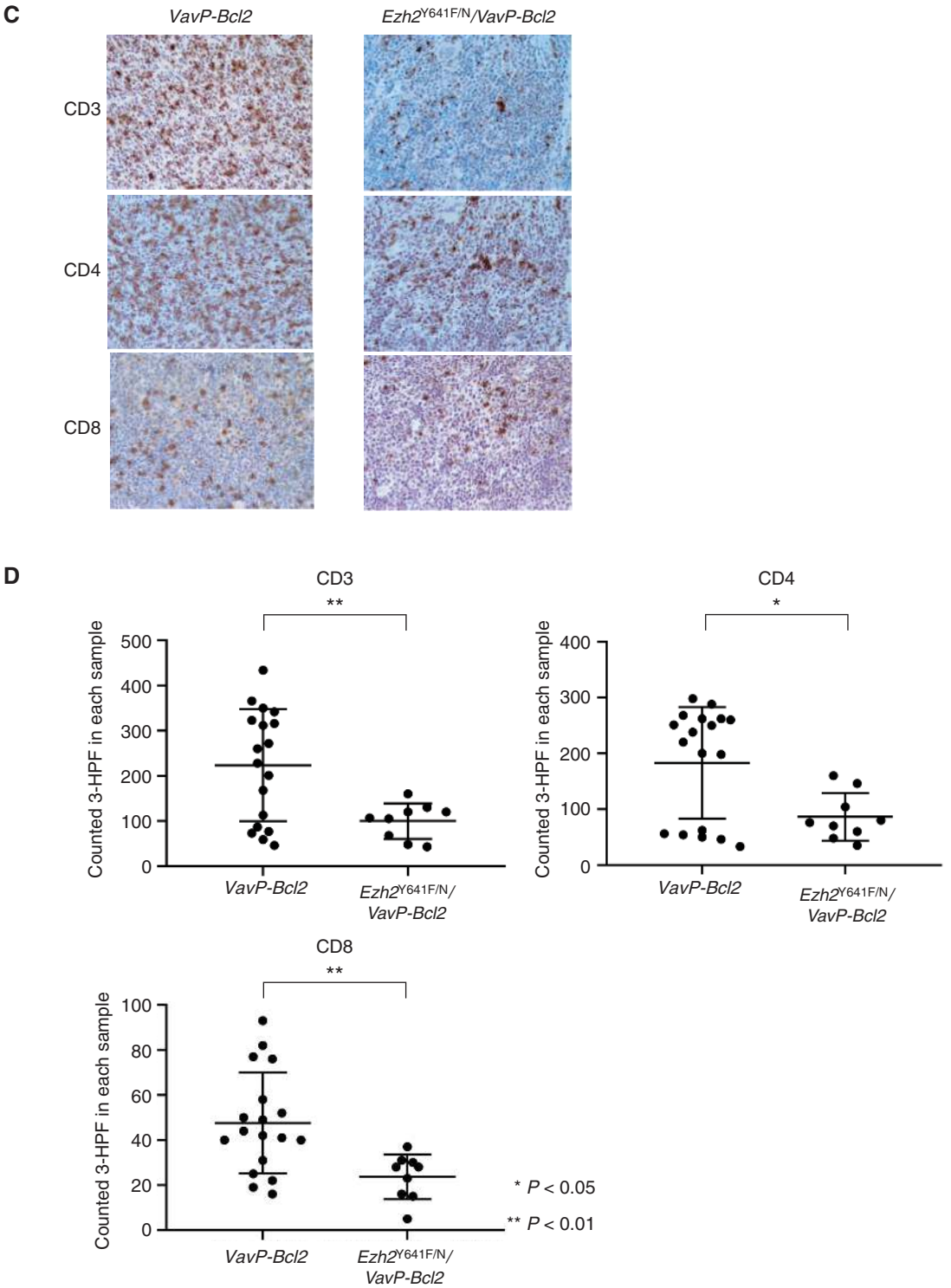

Figure 6. ***(Continued)*** **C,** Tissues from *Ezh2* WT/*VavP-Bcl2* and *Ezh2*$^{Y641F/N}$/*VavP-Bcl2* mice were stained with CD3, CD4, and CD8 (magnification, ×40). **D,** Comparison of proportions of CD3-, CD4-, and CD8-positive cells between *Ezh2* WT/*VavP-Bcl2* and *Ezh2*$^{Y641F/N}$/*VavP-Bcl2* mice.

an immune-"cold" microenvironment induced by MHC deficiency. These mice were also observed for survival and tumor development. *VavP-Bcl2* and Cγ1Cre; *Ezh2*$^{Y641F/N}$/*VavP-Bcl2* showed an accelerated lethal phenotype, with deaths due to progressive lymphoma beginning at day 180, whereas Cγ1Cre; *Ezh2*$^{Y641F/N}$ mice began to die at day 500 (Supplementary Fig. S5A). Macroscopic examination of spleens also showed marked splenomegaly in *VavP-Bcl2* and

Cγ1Cre; *Ezh2*$^{Y641F/N}$/*VavP-Bcl2* (Supplementary Fig. S5B). Collectively, we confirmed the MHC deficiency induced by *Ezh2* mutation, which generates an immune-"cold" environment, in two independent *in vivo* model systems.

EZH2 Mutation Is Identified as a Therapeutic Target for Restoring MHC Expression

Next, we examined whether EZH2 inhibitor treatment restores MHC expression in human DLBCL cells harboring *EZH2* mutations. First, we confirmed that the EZH2 inhibitor EPZ-6438 depleted H3K27me3 in DLBCL cell lines (Supplementary Fig. S6A and S6B). Of importance, treatment with EPZ-6438 significantly increased surface MHC-I protein expression in all *EZH2*-mutant GCB-type cell lines except WSU-DLCL2. No change of MHC-I expression was observed in *EZH2* WT DOHH-2, SU-DHL-8, and TOLEDO cells (Fig. 7A and B). Although most cell lines tested were not totally deficient for MHC-I expression at baseline, EZH2 inhibitor treatment could increase MHC-I expression to significantly higher expression levels in *EZH2*-mutant cells (Supplementary Fig. S7A and S7B). Similarly, significant elevation of MHC-II expression was also observed in *EZH2*-mutant SU-DHL4, WSU-DLCL2, and SU-DHL-10 cells, whereas no differences of surface MHC-II levels were seen in *EZH2* WT DLBCL cells (Fig. 7A–C).

To characterize in more detail the function of *EZH2* mutations in mature B cells, we analyzed chromatin immunoprecipitation sequencing (ChIP-seq) data of murine BCL1 cells transduced to express either *EZH2*^{Y641} mutants or WT *EZH2* and focused on NLRC5 and CIITA, which are known as the MHC-I and MHC-II transactivators, respectively. BCL1 cells, which are an established model to study GC B-cell biology (28), transduced with *EZH2*^{Y641N} and *EZH2*^{Y641F} exhibited increased H3K27me3 levels at promoters of *Nlrc5* and *Ciita* compared with WT *EZH2* (Supplementary Fig. S8). In addition, we examined whether EZH2 inhibition induces the restoration of *NLRC5* and *CIITA* in human DLBCL cells. RT-PCR analysis revealed that treatment with EPZ-6438 led to a significant increase of *NLRC5* in all mutant cell lines ($P < 0.05$; Fig. 7D), whereas its expression was only marginally increased in *EZH2* WT cells. We also observed significant upregulation of *CIITA* in all mutant cell lines, but not in *EZH2* WT cells. Furthermore, ChIP-seq data showed that the EZH2 inhibitor GSK343 decreased H3K27me3 levels at promoters of *NLRC5* and *CIITA* in the *EZH2*-mutant DLBCL cell line SU-DHL-6 compared with control compound (GSK669), whereas this reduction was not observed in the *EZH2* WT cell line OCI-Ly7 (Fig. 7E).

Overall, these results demonstrate that EZH2 epigenetically regulates the MHC system through transcriptional repression of MHC-I/II transactivators. Moreover, we show that EZH2 inhibitors can restore MHC expression preferentially in *EZH2* mutation–carrying cells.

DISCUSSION

Cancer cells frequently manifest downregulation of MHC expression on the cell surface, losing the ability to present antigen and allowing tumors to escape from tumor-infiltrating immune cells (1, 2). Hence, identification of molecular aberrations responsible for altered tumor MHC expression, as well as understanding the evolution of this expression during the course of tumor development, becomes essential for the success of T cell–mediated cancer immunotherapy. Moreover, the cells of origin of B-cell lymphomas are themselves professional APCs; thus, the mechanism and outcome of MHC deficiency may be different from those of solid tumors. In this study, we have comprehensively analyzed the genetic and molecular basis of loss of MHC-I and MHC-II expression, as well as their correlates with immune-cell composition in DLBCL. Gene expression profiling demonstrated that MHC-II expression is strongly correlated with transcriptomic changes of the pathways involved in the transition of GC B cells between DZ and LZ, indicating that MHC-II expression can be used as a surrogate for COO derivation from centrocytes and centroblasts. In addition, the cases with MHC-II loss show a significantly lower amount of TILs and lower cytolytic activity, which may explain the worse treatment outcome compared with MHC-II–positive cases.

Our reported associations of MHC-II expression with disease biology and treatment outcome specifically occurred in GCB-DLBCL, reflecting a substantial degree of dependence on microenvironmental cells for survival and proliferation signals in the GC. Normal centroblasts and centrocytes themselves display an expression gradient of surface MHC-II expression during B-cell differentiation (21, 26). Our findings suggest a scenario where DZ B cells or DZ B cells in transition to LZ phenotypes selectively gain *CIITA, RFXAP,* and *EZH2* mutations during tumor development to maintain or further reduce MHC-II expression levels. On the other hand, LZ B cells with relatively high MHC-II expression might acquire genetic aberrations to maintain or further increase MHC-II expression (Fig. 3B). This suggests a tumor progression model of acquired immune escape by skewing the cross-talk with effector T cells in GC-derived lymphomas with MHC-II deficiency. Notably, previous studies also demonstrated that *CREBBP* mutations downregulate MHC-II expression which results in reduced T-cell infiltration in follicular lymphoma and GCB-DLBCL, but not in ABC-DLBCL (29, 30). This model is also in contrast to that of solid cancers, where selective pressure imposed by cytotoxic T cells gave growth advantage to tumor cells that have lost the ability to effectively present antigen (8, 31).

Our genetic study using a large population-based cohort allowed us to perform precise molecular mapping of recurrent genetic alterations underlying loss of MHC expression. This analysis highlighted that *EZH2*-mutant DLBCL cases have both significantly lower MHC-I and MHC-II expression compared with *EZH2* WT tumors. *EZH2*, which encodes the catalytic component of the polycomb repressor complex 2, is one of the most frequently mutated genes in human lymphomas, especially GC-derived lymphomas, accounting for 27% of patients with follicular lymphoma and 30% of patients with GCB-DLBCL (32, 33). *EZH2* mutations drive lymphomagenesis by repressing target genes involved in proliferation checkpoints (e.g., *CDKN1A*) and B-cell terminal differentiation (e.g., *IRF4* and *PRDM1*; refs. 27, 34). In addition to these "intrinsic"

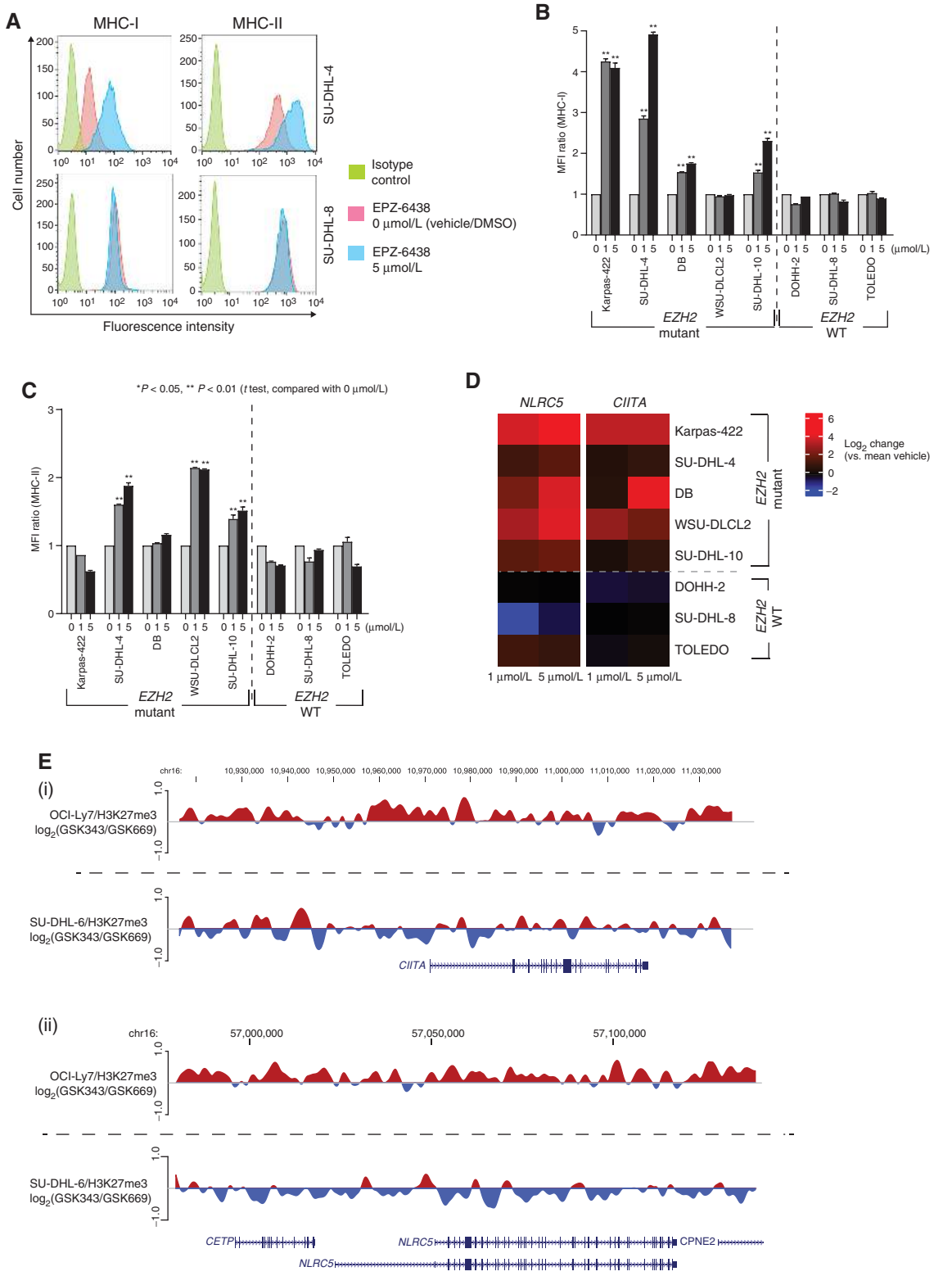

Figure 7. Restoration of MHC expression by EZH2 inhibitors in human DLBCL cells with *EZH2* Y641 mutations. **A,** Representative flow cytometry results of MHC-I and MHC-II surface expression change in SU-DHL-4 and SU-DHL-8 treated by EPZ-6438. **B** and **C,** Summary of MHC-I and MHC-II flow cytometry for Karpas-422, SU-DHL-4, DB, WSU-DLCL2 and SU-DHL-10 (*EZH2* mutant) and DOHH-2, SU-DHL-8, and TOLEDO (*EZH2* WT) cells treated by EPZ-6438 with different concentrations. *, $P < 0.05$; **, $P < 0.01$ (*t* test, compared with 0 μmol/L). **D,** Heat map shows *NLRC5* and *CIITA* differential expression (log_2 ratio, standardized by GAPDH) in *EZH2* mutant and WT cell lines treated with EPZ-6438 (vehicle, 1 μmol/L and 5 μmol/L). Red, elevated; blue, decreased expression compared with vehicle control. **E,** Comparisons of H3K27me3 ChIP-seq read density treated with GSK343 or GSK669 (compound control) at *CIITA* (i) and *NLRC5* (ii) gene loci in OCI-LY7 cells (*EZH2* WT, top) or SU-DHL-6 cells (*EZH2* Y641 mutation, bottom).

pathways, our study demonstrates their "extrinsic" effects to drive lymphoma development. Previous studies showed that *EZH2* mutations may mediate MHC-II expression through downregulation of *CIITA*, which is the master regulator of MHC-II genes (35). In addition, NLRC5 has been recently identified as a transactivator of MHC class I, which was shown to regulate MHC-I expression by reducing H3K27me3 on the MHC-I promoter (10, 36). As shown in several previous publications, the expression levels of *NLRC5* and MHC-I are highly correlated, with more NLRC5 resulting in higher MHC-I expression and increased MHC-I cell surface levels (10, 37). Similarly, *CIITA* expression and MHC-II surface levels were also known to be significantly correlated (38, 39). Moreover, downregulation of *NLRC5* and *CIITA* was reported to lead to a reduction in TILs (10, 40). Therefore, our results demonstrate the upregulation of *NLRC5* and *CIITA* in *EZH2*-mutated DLBCL cells treated with EZH2 inhibitors and provide an explanation for the specificity of these mutations to DLBCL with MHC deficiency.

Of clinical importance, our study shows that EZH2 inhibitor treatment restores MHC-I and MHC-II expression on *EZH2*-mutant DLBCL cells. Tazemetostat (EPZ-6438) has shown strong antilymphoma activity in a recent clinical trial (41), and therefore this restoration might elicit additional effects based on potent antitumor immunity associated with increased T-cell infiltration in MHC-I– and MHC-II–negative tumors. Especially, we observed an increased amount of TILs as well as upregulation of immune-checkpoint markers, especially PDCD1 and CTLA4 in MHC-II–positive cases, thus providing a rationale for novel combination strategies of targeting EZH2 with immune-checkpoint inhibitors. Importantly, recent studies on the role of epigenetics in immune evasion have exposed a key role for epigenetic modulators in augmenting the tumor microenvironment and restoring immune recognition and immunogenicity. For example, an attractive strategy for the restoration of MHC expression has been described, including epigenetic modifiers, like inhibitors of histone deacetylases (HDAC) or DNA methyltransferases (DNMT), where such regulation at the epigenetic level was shown to be able to synergize with immunotherapy for the eradication of mouse tumor models (42, 43). Notably, the inhibition of HDAC3 can restore MHC class II expression, which was reported to be suppressed in *CREBBP*-mutant B-cell lymphoma models (29). A recent study has also demonstrated that *EZH2* and *DNMT1* gene expression was negatively correlated with the amount of TILs through silencing of Th1-type chemokines (44). Collectively, these studies and our data strongly suggest the potential of epigenetic reprogramming for priming the host immune system to immunotherapies in a subset of DLBCLs.

In conclusion, the integration of transcriptomic, genetic, and immunophenotypic data has revealed a key role of MHC expression to define distinct biological and immunologic phenotypes in a COO-dependent manner. These results inform on how MHC-deficient lymphoid tumors evolve with tumor-preferable microenvironments, which affect clinical outcome in DLBCL. We highlight that acquired MHC deficiency is frequently observed in *EZH2*-mutated lymphomas, in which EZH2 inhibitors can restore MHC expression, thus paving the way for novel combination immunotherapies simultaneously treating the tumor and host immunity.

METHODS

Detailed materials and methods are available in the supplementary data.

Patient Cohort Description

Initially, the British Columbia Cancer (BC Cancer) Lymphoid Cancer database was searched to identify all patients with DLBCL diagnosed between 1985 and 2011. From 4,063 DLBCL cases, 347 patients with *de novo* DLBCL were included in the final cohort for analysis if they met the following criteria: Patients had to be 16 years of age or older, treated uniformly with R-CHOP with curative intent at BC Cancer, had complete clinical, laboratory, and outcome data available, and had a fresh-frozen diagnostic biopsy. The diagnosis was made according to the 2008 World Health Organization classification, as determined by standardized review by expert hematopathologists (A. Mottok, P. Farinha, and R.D. Gascoyne). Patients were excluded if they had any of the following: primary mediastinal large B-cell lymphoma; primary or secondary central nervous system involvement at diagnosis; a previous diagnosis of an indolent lymphoproliferative disorder; positive HIV serology; a secondary malignancy; or major medical comorbidity that precluded treatment with curative intent. As described previously, the baseline characteristics and outcomes in the study cohort were similar to those of the entire population of patients with DLBCL (n = 1,177) treated with curative intent in BC during that time, with the exception that there was a significantly lower proportion of patients with two or more extranodal sites in the study cohort (45).

This study was reviewed and approved by the University of British Columbia-BC Cancer Research Ethics Board, in accordance with the Declaration of Helsinki. Informed consent was waived for the samples used in this retrospective study by the University of British Columbia-BC Cancer Research Ethics Board (H14-02304).

IHC on TMA and COO Assignment

For IHC staining, 4-μm slides of the TMAs of 341 DLBCL cases and mouse tumor specimens (7 *VavP-Bcl2* and 3 *Ezh2*$^{Y641F/N}$/*VavP-Bcl2* mice), and antibodies listed in Supplementary Table S11, were used. Unless otherwise stated, staining was performed on a Benchmark XT platform (Ventana). IHC for anti-mouse CD3, CD4, CD8 was performed according to the manufacturer's instructions. The protein expression of MHC-I and MHC-II was recorded semiquantitatively: negative; cytoplasmic expression; or membranous expression in tumor cells. As for the MHC-I and MHC-II expression in mouse tissues (*VavP-Bcl2* and *Ezh2*^{Y641N}/*VavP-Bcl2*), proportion of positive tumor cells was calculated by at least one expert hematopathologist (K. Takata and/or P. Farinha). Immunohistochemically stained slides for the T-cell markers CD4, CD8, FOXP3, and PD-1, GATA3, and T-bet as well as the macrophage markers CD68 and CD163 were scanned with an Aperio ScanScope XT at 20x magnification. Image analysis was performed using the Aperio ImageScope viewer (v12.1.0; Aperio Technologies). The Positive Pixel Count algorithm with an optimized color saturation threshold was then applied to tumor-containing areas, and any staining was considered positive. The number of positive pixels was divided by the total pixel count and multiplied by 100 to obtain the percentage of positive pixels. Representative images were taken using a Nikon Eclipse 80i microscope equipped with a Nikon DS-Ri1 camera and NIS Elements Imaging Software, D3.10.

Digital gene expression profiling (GEP) was performed to assign COO using a Lymph2Cx 20-gene GEP assay on the NanoString platform (NanoString Technologies) for 327 cases with a tumor content

>10% based on histologic evaluation of formalin-fixed, paraffin-embedded tissue (FFPET) biopsy sections (45, 46). Based on these procedures, COO was successfully assigned in 323 cases. One hundred eighty-three cases were assigned to the GCB subtype, 104 cases were ABC, and 36 were unclassified.

Flow Cytometry Analysis

Flow cytometric immunophenotyping was performed on cell suspensions from freshly disaggregated lymph node biopsies using a routine diagnostic panel and stained according to the manufacturer's recommendations with CD3, CD4, and CD8 monoclonal antibodies (Beckman Coulter). Analysis was performed on a Cytomics FC 500 flow cytometer (samples processed between 1985 and 2009; Beckman Coulter) or BD FACS Canto (samples processed between 2009 and 2011; BD Biosciences).

Targeted Sequencing

Mutational data were generated based on deep-targeted sequencing using the TruSeq Custom Amplicon assay (TSCA; mean coverage: 767; range: 128–2,039; SD: 180). For the validation of detected variants, we also performed deep-targeted sequencing with Fluidigm Access Array system. We sequenced the protein-coding regions of 59 genes in 347 tumors and 67 matched normal samples using deep-targeted sequencing. The procedures of gene selection and library construction were previously described (29, 45, 47). Samtools-0.1.19 was used by the pipeline to create the pileup files and dbsnp137 for SNP annotation. For normal specimens, we pooled BAM files of 67 normal controls and created quasinormal data. In the final list, all variants with an allele frequency of ≥5% at loci covered by at least 50-fold were retained. Two genes were removed at this stage due to poor sequence coverage and quality in >80% samples, *HLA-C* and *TLCS*, leaving a total of 57 genes for further analysis. We used two orthogonal deep-sequencing strategies (Fluidigm Array and TSCA) for the validation of single-nucleotide variants and indels and achieved a 97% validation rate. The detailed procedures of gene selection, library construction, and filtering are shown in the supplementary material and have been described previously (29, 45, 47).

SNP6.0-Based Copy-Number Analysis

DNA samples from 341 DLBCL cases were analyzed with Affymetrix Human SNP6.0 Arrays (Affymetrix). Library construction and data processing are described in the supplementary material. Briefly, copy-number segments and gene-centric copy-number states were generated using OncoSNP as previously described (45). GISTIC (v2.0.12) was also run on the OncoSNP-segmented data to identify minimally commonly deleted and amplified regions. Then, we selected GISTIC regions and used ONCOSNIP category data for further analysis.

Using these mutation and copy-number alteration (CNA) data, enrichment of genetic alterations between MHC-positive and MHC-negative cases was assessed using the Fisher exact test (Supplementary Tables S4 and S5). We also evaluated the recurrent genetic alterations in MHC-I and MHC-II double-positive cases (Supplementary Tables S12–S14) and MHC cytoplasmic-positive cases (Supplementary Fig. S9; detailed information is shown in supplementary material).

RNA-seq Analysis

We obtained RNA-seq data for 322 DLBCL samples to quantify the gene expression levels. Library construction is described in the supplementary material. Pooled libraries were sequenced as paired-end 75 bp on the Hiseq 2500 platform. This yielded, on average, 71 million reads per patient (range, 6.5–163.7 million reads). Paired end RNA-seq FASTQ files were used as input to our differential analysis pipeline starting with alignment using the STAR aligner (STAR_2.5.1b_modified). The nondefault parameters were chosen as recommended by the STAR-Fusion guidelines (https://github.com/STAR-Fusion/STAR-Fusion/wiki), as the same aligned reads were also used for STAR-Fusion gene fusion analysis. Detailed data analysis was previously described (47).

GSEA and PEA Analysis

Enrichment of upregulated gene signatures of DZ and LZ (21) was assessed using the GSEA algorithm against a gene list preranked for $\log_2$ ratio of expression from MHC-II–negative samples to expression from MHC-II–positive samples. The statistics provided for GSEA (including *P* value, normalized *P* value, and FDR) were calculated by the GSEA software Version 3.0. PEA and subsequently construction of a gene interaction network was performed for significantly upregulated and downregulated genes (fold change, <–1 or >+1, and adjusted *P* value < 0.01) according to MHC-II expression status using the ReactomeFI plugin (v4.1.1. beta) in CytoScape (v3.2.1).

Evaluation of the Immune-Cell Fraction Based on Gene Expression Profiling

For the evaluation of the immune-cell fractions, we ran CIBERSORT using our RNA-seq data according to the manual (https://cibersort.stanford.edu). We used the LM22 signature gene file for the reference gene signatures as described previously (48).

Survival Analysis

The Kaplan–Meier method was used to estimate the TTP (progression/relapse or death from lymphoma or acute treatment toxicity) and overall survival (death from any cause), with the log-rank test performed to compare survival curves. In this study, we mainly used TTP to reflect the direct influence of genetic features on tumor progression without the confounding of death events unrelated to lymphoma. Univariate and multivariate Cox proportional hazard regression models were used to evaluate proposed prognostic factors.

Cell Lines and Mouse Tissues

Human DLBCL cell lines Karpas-422, SU-DHL-4, WSU-DLCL2, SU-DHL-10, DB, DOHH-2, and SU-DHL-8 were purchased from DSMZ. TOLEDO cell lines were purchased from the ATCC. Karpas-422, SU-DHL-4, SU-DHL-10, SU-DHL-8, and DB were cultured in RPMI-1640 (Thermo Fisher Scientific) supplemented with 20% FBS (Thermo Fisher Scientific), and WSU-DLCL2, DOHH-2, and TOLEDO were cultured in RPMI-1640 supplemented with 10% FBS. All cell lines have been confirmed to be negative for *Mycoplasma* before culture using VenorTMGeM Mycoplasma Detection Kit, PCR-based (Sigma, MP0025). All cell lines were authenticated by short tandem repeat profiling (The Centre for Applied Genomics, The Hospital for Sick Children, Toronto, Canada; Supplementary Table S15). Mutations in *EZH2*, HLA-ABC, and HLA-DP/DQ/DR in the cell lines were evaluated using the COSMIC (https://cancer.sanger.ac.uk/cosmic) databases.

FFPET were obtained from conditional *EZH2*^{Y641}/*BCL2* transgenic mice.

Murine Models

The Research Animal Resource Center of the Weill Cornell Medical College of Medicine approved all mouse procedures. Conditional *Ezh2*^{Y641F} knock-in and transgenic *Ezh2*^{Y641N} mice were generated as described previously (27, 34). By crossing floxed *Ezh2*$^{Y641F/N}$ with the transgenic Cγ cre strain (The Jackson Laboratory, 010611), we generated heterozygous mice, which were crossed to *VavP-Bcl2* transgenic animals (49).

Treatment with EZH2 Inhibitors, FACS Analysis for MHC, and Immunoblotting

DLBCL cell lines were grown in 24-well plates, and cell viability was determined using the trypan blue automatic method (Countess II

FL automated cell counter, Thermo Fisher Scientific). DLBCL cell lines were exposed at 3 concentrations (in DMSO: 0 μmol/L, 1 μmol/L, 5 μmol/L) of tazemetostat (EPZ-6438) for 7 days and analyzed for cell viability as before. Cells were seeded in triplicate (100,000 cells/mL) and split every 3 to 4 days as previously described (27, 50). After 7 days of treatment, cells were stained using the following fluorescent-labeled anti-human antibodies: FITC-conjugated anti–HLA-ABC, FITC-conjugated anti-human HLA-DR/DP/DQ, mouse IgG1 K isotype control, mouse IgG2a K isotype control (all from BD Biosciences). Data were acquired on FACSCalibur (BD Biosciences) and analyzed using FlowJo software (ver. 10). Mean fluorescent intensity (MFI) was calculated in triplicate samples, and the MFI ratio was calculated in comparison to the DMSO control. RIPA buffer (Thermo Scientific) was used to extract protein following the manufacturer's instructions. The immunoblot experiments were performed with standard procedures. Blots were stained with anti-H3K27me3 (Lys27, C36B11, Cell Signaling Technology) following the manufacturer's instructions. GAPDH (MAB374, Millipore) was included as an internal loading control.

qRT-PCR Analysis

RNA was extracted using RNeasy Mini Kits (Qiagen, 74106). qRT-PCR assays (Applied Biosystems) were used for *NLRC5* and *CIITA* expression using predesigned probes for *NLRC5* (Hs1072123_m1), *CIITA* (Hs00172106_m1), and *GAPDH* (Thermo Fisher Scientific, 4332649). Each assay was replicated 3 times, and *NLRC5* and *CIITA* gene expression was normalized using *GAPDH* gene expression (ΔΔCT method). Fold change was calculated compared with DMSO (0 μmol/L) samples. ComplexHeatmap R package version 1.17.1 was used to visualize tazemetostat (EPZ-6438)-induced changes in *NLRC5* and *CIITA* transcript levels.

Statistical Comparisons

The Fisher exact test was used when comparing two categorical variables. For the comparison of two continuous variables, these data were tested by Wilcoxon rank-sum tests, unless otherwise noted. Multiple testing correction was performed, where necessary, using the Benjamini–Hochberg procedure. All quantitative results are presented as the mean with SD. The statistical significance of the differences between cell culture groups was determined using the Student *t* tests. Primary cell comparisons were analyzed with two-way repeated measure ANOVA with Bonferroni multiple comparisons test. All reported *P* values were two-sided, and those <0.05 were considered statistically significant. All statistical analyses were performed using R software v3.2.3 and GraphPad Prism Version 7 (GraphPad Software Inc.).

Disclosure of Potential Conflicts of Interest

L.H. Sehn reports receiving honoraria from the speakers' bureaus of Roche/Genentech, Janssen, Celgene, Apobiologix, AstraZeneca, Acerta, Takeda, TG Therapeutics, Teva, Kite, Merck, Amgen, Seattle Genetics, AbbVie, Morphosys, Karyopharm, Lundbeck, and Gilead. S.P. Shah has ownership interest (including stock, patents, etc.) in Contextual Genomics Inc. and is a consultant/advisory board member for the same. D.W. Scott reports receiving commercial research grants from Roche/Genentech, NanoString Technologies, and Janssen; and is a consultant/advisory board member for Janssen and Celgene. A.M. Melnick reports receiving commercial research grants from Janssen and GSK; has ownership interest (including stock, patents, etc.) in KDAC; and is a consultant/advisory board member for Janssen. C. Steidl reports receiving a commercial research grant from Bristol-Myers Squibb and is a consultant/advisory board member for Seattle Genetics and Roche. British Columbia Cancer has ownership interest in a patent licensed to NanoString technologies. No potential conflicts of interest were disclosed by the other authors.

Authors' Contributions

Conception and design: D. Ennishi, K. Takata, R.D. Gascoyne, D.W. Scott, A.M. Melnick, C. Steidl

Development of methodology: D. Ennishi, K. Takata, S. Saberi, S. Ben-Neriah

Acquisition of data (provided animals, acquired and managed patients, provided facilities, etc.): D. Ennishi, K. Takata, W. Béguelin, A. Mottok, S. Saberi, M. Boyle, B.W. Woolcock, R. Kridel, K.J. Savage, L.H. Sehn, R.D. Morin, M.A. Marra, J.M. Connors, R.D. Gascoyne, D.W. Scott, A.M. Melnick, C. Steidl

Analysis and interpretation of data (e.g., statistical analysis, biostatistics, computational analysis): D. Ennishi, K. Takata, G. Duns, A. Mottok, P. Farinha, A. Bashashati, S. Saberi, D. Lai, M. Teater, R. Kridel, L.H. Sehn, R.D. Morin, S.P. Shah, J.M. Connors, R.D. Gascoyne, D.W. Scott, A.M. Melnick, C. Steidl

Writing, review, and/or revision of the manuscript: D. Ennishi, K. Takata, W. Béguelin, G. Duns, A. Mottok, P. Farinha, M. Boyle, S. Ben-Neriah, M. Teater, R. Kridel, K.J. Savage, L.H. Sehn, M.A. Marra, J.M. Connors, R.D. Gascoyne, D.W. Scott, A.M. Melnick, C. Steidl

Administrative, technical, or material support (i.e., reporting or organizing data, constructing databases): M. Boyle, B. Meissner, B.W. Woolcock, A. Telenius, A.M. Melnick, C. Steidl

Study supervision: R.D. Gascoyne, D.W. Scott, C. Steidl

Acknowledgments

This study was supported by a Program Project Grant from the Terry Fox Research Institute (R.D. Gascoyne, Grant No. 1023; C. Steidl, Grant No. 1061). D. Ennishi was supported by fellowships from the Michael Smith Foundation for Health Research (MSFHR), Canadian Institutes of Health Research (CIHR), and the Japanese Society for The Promotion of Science. K. Takata was supported by fellowships from The Uehara Memorial Foundation. D.W. Scott is supported by the British Columbia Cancer Foundation (BCCF). J.M. Connors and C. Steidl received research funding support from the Terry Fox Research Institute, Genome Canada, Genome British Columbia, CIHR, and the BCCF. A. Mottok was supported by fellowships from the Mildred-Scheel-Cancer-Foundation (German Cancer Aid), the MSFHR, and Lymphoma Canada. R.D. Morin was funded by a CIHR New Investigator Award. M.A. Marra was pleased to acknowledge support from CIHR (FDN-143288) and the Terry Fox Research Institute. S. Shah holds the Canada Research Chair in Computational Cancer Genomics, is an MSFHR scholar, holds a CIHR Foundation grant, and acknowledges support from the BCCF. C. Steidl is supported by a Michael Smith Foundation for Health Research Investigator award.

The costs of publication of this article were defrayed in part by the payment of page charges. This article must therefore be hereby marked *advertisement* in accordance with 18 U.S.C. Section 1734 solely to indicate this fact.

Received September 20, 2018; revised December 21, 2018; accepted January 28, 2019; published first January 31, 2019.

REFERENCES

1. Hanahan D, Weinberg RA. Hallmarks of cancer: the next generation. Cell 2011;144:646–74.
2. Vinay DS, Ryan EP, Pawelec G, Talib WH, Stagg J, Elkord E, et al. Immune evasion in cancer: mechanistic basis and therapeutic strategies. Semin Cancer Biol 2015;35:S185–98.
3. Ardolino M, Azimi CS, Iannello A, Trevino TN, Horan L, Zhang L, et al. Cytokine therapy reverses NK cell anergy in MHC-deficient tumors. J Clin Invest 2014;124:4781–94.

4. Schumacher TN, Schreiber RD. Neoantigens in cancer immunotherapy. Science 2015;348:69–74.
5. Topalian SL, Drake CG, Pardoll DM. Immune checkpoint blockade: a common denominator approach to cancer therapy. Cancer Cell 2015;27:450–61.
6. Miller JFAP, Sadelain M. The journey from discoveries in fundamental immunology to cancer immunotherapy. Cancer Cell 2015;27:439–49.
7. Garrido F, Aptsiauri N, Doorduijn EM, Garcia Lora AM, van Hall T. The urgent need to recover MHC class I in cancers for effective immunotherapy. Curr Opin Immunol 2016;39:44–51.
8. McGranahan N, Rosenthal R, Hiley CT, Rowan AJ, Watkins TBK, Wilson GA, et al. Allele-specific HLA loss and immune escape in lung cancer evolution. Cell 2017;171:1259–71.e11.
9. Kreiter S, Vormehr M, van de Roemer N, Diken M, Löwer M, Diekmann J, et al. Mutant MHC class II epitopes drive therapeutic immune responses to cancer. Nature 2015;520:692–6.
10. Yoshihama S, Roszik J, Downs I, Meissner TB, Vijayan S, Chapuy B, et al. NLRC5/MHC class I transactivator is a target for immune evasion in cancer. Proc Natl Acad Sci 2016;113:5999–6004.
11. Challa-Malladi M, Lieu YK, Califano O, Holmes AB, Bhagat G, Murty V V, et al. Combined genetic inactivation of β2-Microglobulin and CD58 reveals frequent escape from immune recognition in diffuse large B cell lymphoma. Cancer Cell 2011;20:728–40.
12. Rimsza LM, Roberts RA, Campo E, Grogan TM, Bea S, Salaverria I, et al. Loss of major histocompatibility class II expression in non-immune-privileged site diffuse large B-cell lymphoma is highly coordinated and not due to chromosomal deletions. Blood 2006;107:1101–7.
13. Rimsza LM, Roberts RA, Miller TP, Unger JM, LeBlanc M, Braziel RM, et al. Loss of MHC class II gene and protein expression in diffuse large B-cell lymphoma is related to decreased tumor immunosurveillance and poor patient survival regardless of other prognostic factors: a follow-up study from the leukemia and lymphoma molecular. Blood 2004;103:4251–8.
14. Alizadeh AA, Eisen MB, Davis RE, Ma C, Lossos IS, Rosenwald A, et al. Distinct types of diffuse large B-cell lymphoma identified by gene expression profiling. Nature 2000;403:503–11.
15. Shipp MA, Ross KN, Tamayo P, Weng AP, Kutok JL, Aguiar RCT, et al. Diffuse large B-cell lymphoma outcome prediction by gene-expression profiling and supervised machine learning. Nat Med 2002;8:68–74.
16. Reddy A, Zhang J, Davis NS, Moffitt AB, Love CL, Waldrop A, et al. Genetic and functional drivers of diffuse large B cell lymphoma. Cell 2017;171:481–94.e15.
17. Schmitz R, Wright GW, Huang DW, Johnson CA, Phelan JD, Wang JQ, et al. Genetics and pathogenesis of diffuse large B-cell lymphoma. N Engl J Med 2018;378:1396–407.
18. Chapuy B, Stewart C, Dunford AJ, Kim J, Kamburov A, Redd RA, et al. Molecular subtypes of diffuse large B cell lymphoma are associated with distinct pathogenic mechanisms and outcomes. Nat Med 2018;24:679–90.
19. Wilkinson ST, Vanpatten KA, Fernandez DR, Brunhoeber P, Garsha KE, Glinsmann-Gibson BJ, et al. Partial plasma cell differentiation as a mechanism of lost major histocompatibility complex class II expression in diffuse large B-cell lymphoma. Blood 2012;119:1459–67.
20. Nijland M, Veenstra RN, Visser L, Xu C, Kushekhar K, van Imhoff GW, et al. HLA dependent immune escape mechanisms in B-cell lymphomas: implications for immune checkpoint inhibitor therapy? Oncoimmunology 2017;6:1–8.
21. Victora GD, Dominguez-Sola D, Holmes AB, Deroubaix S, Dalla-Favera R, Nussenzweig MC. Identification of human germinal center light and dark zone cells and their relationship to human B-cell lymphomas. Blood 2012;120:2240–8.
22. Klein U, Tu Y, Stolovitzky GA, Keller JL, Haddad J, Miljkovic V, et al. Transcriptional analysis of the B cell germinal center reaction. Proc Natl Acad Sci 2003;100:2639–44.
23. Green B, Belcheva A, Nepal RM, Boulianne B, Martin A. The mismatch repair pathway functions normally at a non-AID target in germinal center B cells. Blood 2011;118:3013–8.
24. Rimsza LM, Chan WC, Gascoyne RD, Campo E, Jaffe ES, Staudt LM, et al. CIITA or RFX coding region loss of function mutations occur rarely in diffuse large b-cell lymphoma cases and cell lines with low levels of major histocompatibility complex class ii expression. Haematologica 2009;94:596–8.
25. Mottok A, Woolcock B, Chan FC, Tong KM, Chong L, Farinha P, et al. Genomic alterations in CIITA are frequent in primary mediastinal large B cell lymphoma and are associated with diminished MHC class II expression. Cell Rep 2015;13:1418–31.
26. Bannard O, McGowan SJ, Ersching J, Ishido S, Victora GD, Shin J-S, et al. Ubiquitin-mediated fluctuations in MHC class II facilitate efficient germinal center B cell responses. J Exp Med 2016;213:993–1009.
27. Béguelin W, Popovic R, Teater M, Jiang Y, Bunting KL, Rosen M, et al. EZH2 is required for germinal center formation and somatic EZH2 mutations promote lymphoid transformation. Cancer Cell 2013;23:677–92.
28. Blackman MA, Tigges MA, Minie ME, Koshland ME. A model system for peptide hormone action in differentiation: interleukin 2 induces a B lymphoma to transcribe the J chain gene. Cell 1986;47:609–17.
29. Jiang Y, Ortega-Molina A, Geng H, Ying H-Y, Hatzi K, Parsa S, et al. CREBBP inactivation promotes the development of HDAC3-Dependent Lymphomas. Cancer Discov 2017;7:38–53.
30. Green MR, Kihira S, Liu CL, Nair RV, Salari R, Gentles AJ, et al. Mutations in early follicular lymphoma progenitors are associated with suppressed antigen presentation. Proc Natl Acad Sci U S A 2015;112:E1116–25.
31. Rooney MS, Shukla Sa, Wu CJ, Getz G, Hacohen N. Article molecular and genetic properties of tumors associated with local immune cytolytic activity. Cell 2014;160:48–61.
32. Morin RD, Johnson NA, Severson TM, Mungall AJ, An J, Goya R, et al. Somatic mutations altering EZH2 (Tyr641) in follicular and diffuse large B-cell lymphomas of germinal-center origin. Nat Genet 2010;42:181–5.
33. Pasqualucci L, Trifonov V, Fabbri G, Ma J, Rossi D, Chiarenza A, et al. Analysis of the coding genome of diffuse large B-cell lymphoma. Nat Genet 2011;43:830–7.
34. Béguelin W, Teater M, Gearhart MD, Calvo Fernández MT, Goldstein RL, Cárdenas MG, et al. EZH2 and BCL6 cooperate to assemble CBX8-BCOR complex to repress bivalent promoters, mediate germinal center formation and lymphomagenesis. Cancer Cell 2016;30:197–213.
35. Abou El Hassan M, Yu T, Song L, Bremner R. Polycomb repressive complex 2 confers BRG1 dependency on the CIITA locus. J Immunol 2015;194:5007–103.
36. Jongsma MLM, Guarda G, Spaapen RM. The regulatory network behind MHC class I expression. Molecular Immunology (2017), https://doi.org/10.1016/j.molimm.2017.12.005.
37. Neerincx A, Rodriguez GM, Steimle V, Kufer TA. NLRC5 controls basal MHC class I gene expression in an MHC enhanceosome-dependent manner. J Immunol 2012;188:4940–50.
38. Dunn J, Rao S. Epigenetics and immunotherapy: the current state of play. Mol Immunol 2017;87:227–39.
39. Cycon KA, Mulvaney K, Rimsza LM, Persky D, Murphy SP. Histone deacetylase inhibitors activate CIITA and MHC class II antigen expression in diffuse large B-cell lymphoma. Immunology 2013;140:259–72.
40. Dubrot J, Duraes FV, Potin L, Capotosti F, Brighouse D, Suter T, et al. Lymph node stromal cells acquire peptide–MHCII complexes from dendritic cells and induce antigen-specific CD4 + T cell tolerance. J Exp Med 2014;211:1153–66.
41. Italiano A, Soria JC, Toulmonde M, Michot JM, Lucchesi C, Varga A, et al. Tazemetostat, an EZH2 inhibitor, in relapsed or refractory B-cell non-Hodgkin lymphoma and advanced solid tumours: a first-in-human, open-label, phase 1 study. Lancet Oncol 2018;19:649–59.
42. Kim K, Skora AD, Li Z, Liu Q, Tam AJ, Blosser RL, et al. Eradication of metastatic mouse cancers resistant to immune checkpoint blockade by suppression of myeloid-derived cells. Proc Natl Acad Sci 2014;111:11774–9.

43. Chiappinelli KB, Strissel PL, Desrichard A, Li H, Henke C, Akman B, et al. Inhibiting DNA methylation causes an interferon response in cancer via dsRNA including endogenous retroviruses. Cell 2015;162:974–86.
44. Peng D, Kryczek I, Nagarsheth N, Zhao L, Wei S, Wang W, et al. Epigenetic silencing of TH1-type chemokines shapes tumour immunity and immunotherapy. Nature 2015;527:249–53.
45. Ennishi D, Mottok A, Ben-Neriah S, Shulha HP, Farinha P, Chan FC, et al. Genetic profiling of MYC and BCL2 in diffuse large B-cell lymphoma determines cell-of-origin-specific clinical impact. Blood 2017;129:2760–70.
46. Scott DW, Wright GW, Williams PM, Lih C, Walsh W, Jaffe ES, et al. Determining cell-of-origin subtypes of diffuse large B-cell lymphoma using gene expression in formalin-fixed paraffin-embedded tissue. Blood 2014;123:1214–7.
47. Ortega-Molina A, Boss IW, Canela A, Pan H, Jiang Y, Zhao C, et al. The histone lysine methyltransferase KMT2D sustains a gene expression program that represses B cell lymphoma development. Nat Med 2015;21:1199–208.
48. Newman AM, Liu CL, Green MR, Gentles AJ, Feng W, Xu Y, et al. Robust enumeration of cell subsets from tissue expression profiles. Nat Methods 2015;12:453–7.
49. Egle A, Harris AW, Bath ML, O'Reilly L, Cory S. VavP-Bcl2 transgenic mice develop follicular lymphoma preceded by germinal center hyperplasia. Blood 2004;103:2276–83.
50. Brach D, Johnston-Blackwell D, Drew A, Lingaraj T, Motwani V, Warholic NM, et al. EZH2 inhibition by tazemetostat results in altered dependency on B-cell activation signaling in DLBCL. Mol Cancer Ther 2017;16:2586–97.